



Thermal Diffusivity Dependence with Highly Concentrated Graphene Oxide/Water Nanofluids by Mode-Mismatched Dual-Beam Thermal Lens Technique

J. L. Jiménez-Pérez¹ · G. López-Gamboa² · J. F. Sánchez-Ramírez³ · Z. N. Correa-Pacheco⁴ · A. Netzahual-Lopantzi¹ · A. Cruz-Orea⁵

Received: 4 March 2021 / Accepted: 30 April 2021 / Published online: 15 May 2021

© The Author(s), under exclusive licence to Springer Science+Business Media, LLC, part of Springer Nature 2021

Abstract

The thermal properties of graphene oxide (GO) nanoparticles' colloidal suspensions prepared using the microwave-assisted hydrothermal method were determined. The mode-mismatched dual-beam thermal lens technique was employed to measure the thermal diffusivity of GO nanoparticles for different concentrations in the base fluid. By fitting the experimental data to the theoretical expression, the characteristic time constant was determined. The thermal diffusivity of the fluids seemed to be strongly dependent on the presence of the nanoparticles, increasing from $15.02 \pm 0.16 \times 10^{-4} \text{ cm}^2 \cdot \text{s}^{-1}$ to $27.59 \pm 0.51 \times 10^{-4} \text{ cm}^2 \cdot \text{s}^{-1}$ for concentrations ranging from 0.82 %V to 4.00 %V of GO/H₂O. As nanofluids concentration increased, a higher value of thermal diffusivity was obtained. The optical properties, morphology and chemical structure and functional groups of the nanoparticles were characterized by UV–Vis spectroscopy, transmission electron microscopy (TEM) and Fourier Transform infrared spectroscopy (FTIR). Two main absorption peaks at 230 nm and at 303 nm in the UV–Vis spectra were observed. TEM images revealed a uniform size distribution and spherical in shape NPs with mean diameter of 7.4 nm. This novel type of nanofluids have potential applications for heat transfer fluids like solar collectors and heat exchange systems.

Keywords Graphene · Nanofluids · Thermal diffusivity · Thermal lens

✉ J. L. Jiménez-Pérez
jimenezp1957@gmail.com

Extended author information available on the last page of the article

1 Introduction

Photothermal techniques are of special relevance to evaluate the thermophysical properties of fluids. The thermal diffusivity is defined as the rate at which heat transfer into a material having units of $\text{m}^2\cdot\text{s}^{-1}$ and is expressed as $D=k/\rho c_p$, where k is the thermal conductivity, ρ is the mass density and c_p is the specific heat capacity. Several traditional techniques exist to measure these thermal properties, such as photoacoustic [1], pyroelectric [2], photothermal deflection [3], resonant cavity [4], and thermal lens, among others. In this work it is of special importance the thermal lens (TL) technique for which a probe and an excitation laser are used. Their beams are guided collinearly in the opposite direction in the mismatched-mode to measure the thermal diffusivity of several substances such as nanofluids [5–7], paraffin [8], edible oils [9], nanocomposites graphene-based polymers [10], modified TiO_2 nanoparticles and nanofluids that show high energy efficiency in cooling computer systems [11], hybrid nanofluids [12], nanofluids of conductive materials and phase change materials [7, 13], among others. The use of the thermal lens is a very important tool in the thermal characterization of liquids and semitransparent films due to it is a very sensitive, and non-invasive technique. Edible oil, biodiesel and water are for example some of the conventional liquids for heat transfer. However, their efficiency as heat transfer in liquids can be improved. Then, it is necessary to improve their thermal properties. To improve heat transport, metallic nanoparticles are added to fluids such as oil and water. The concentration and dispersion of these particles would improve the thermal properties of the fluid compared to the base liquid, and consequently, the range of applications would be expanded. For example, graphene has high rigidity, outstanding electrical properties, and high thermal conductivity ($3000 \text{ W}\cdot\text{mK}^{-1}$ to $5000 \text{ W}\cdot\text{mK}^{-1}$) in a plane at room temperature. Therefore, is of special interest to use graphene for thermal properties enhancement [10, 14, 15].

Most of the literature, is found to be based in the study of nanofluids' thermal conductivity. It has been reported that the thermal conductivity increases with the increase in the concentration and size of the nanoparticles for nanofluids. For example, it has been found that the thermal conductivity of nanofluids with metal oxide nanoparticles for concentrations higher than 1 % is remarkable increased compared to the base fluid [16]. In addition, in many of the works on the thermal conductivity of nanofluids, different particles such as CNTs and metal oxide particles have been used measuring their thermal properties at room temperature. Ahammed *et al.* [16] showed that the thermal conductivity of graphene in water is influenced by temperature. The percentage of enrichment of thermal conductivity was around 18 %V for 0.17 %V concentration at room temperature measured by hot wire technique. Esfahani *et al.*, [17] reported an enrichment of GO nanosheets of 19.9 % for a concentration of 0.5 wt% in water as the base liquid. In this work, the thermal diffusivity of graphene oxide (GO) in water was measured using the thermal lens technique at room temperature for high concentrations. Until now, no works have been found in the literature, for which this thermal property of GO is reported for higher concentrations. Possible applications of this work lies on of high-performance chillers in solar cells [12] micro-electronics [18], nuclear energy and systems for enhancing forced convective heat transfer [13].

2 Experimental Part

2.1 Samples Preparation

The GO was prepared using the methodology Hummers with some modifications [19]. For the synthesis, 1 g of graphite was added into 23 mL of 98 % H_2SO_4 and stirred at room temperature for 24 h. After that, 100 mg of NaNO_3 was added to the mixture and stirred for 30 min. Subsequently, the mixture was kept below 5 °C using an ice bath, and 3 g of KMnO_4 was slowly added. After heating to 35 °C–40 °C, the mixture was stirred for another 30 min. Then, 46 mL of water was added for 25 min. Then, 140 mL of water and 10 mL of 30 % H_2O_2 were added to stop the reaction. Then, the sample was centrifuged and the synthesized GO at a concentration of 0.5 $\text{mg}\cdot\text{mL}^{-1}$ was dispersed by sonication into individual sheets in distilled water. With the TL technique, it is important to highlight that the samples were sonicated for 50 min to avoid agglomeration of the nanoparticles and the measurement was taken in less than one second. An aqueous dispersion of GO was prepared by chemical reduction of GO using benzylamine. Then, 2 mL of GO aqueous dispersion was added into 4 mL of H_2O and 200 mL of benzylamine were added and the sample was stirred for 30 min at room temperature. After that, the mixture was heated to 90 °C for 90 min. Finally, a dark brown GO dispersion was obtained. The GO nanofluids were stable for 3 months without significant change in the spectral pattern (not shown). Electrostatic interactions and hydrogen bonding between GO and water play a significant role in extraordinary properties of stabilizing in the solution [20].

Concentrations of graphene/water used in this work were 0.82 %V, 1.63 %V, 2.43 %V, and 3.22 %V, 4 %V (Fig. 1). Due to the GO samples are contained in water, the calibration was done with the base liquid. From the expression $t_c = w_e^2/4D$, it is possible to obtain the adjustment parameter t_c to determine the thermal diffusivity. The errors for each concentration, which vary between 1 and 4%, are typical errors in the fit of the theoretical thermal lens equation to the experimental data. Before the measurements, a previous calibration is made to see if similar values are obtained. 10 measurements of the samples were taken and to find the uncertainty of



Fig. 1 Preparation of graphene oxide (GO) for different concentrations 0.82 %V, 1.63 %V, 2.43 %V, and 3.22 %V, 4 %V by the method of Hummers [19]

the thermal diffusivity value $|\Delta D| = D |\Delta t_c / t_c|$, the uncertainty of data depending on one variable procedure was used [21].

2.2 Experimental Set-up

The basic principle of the thermal lens technique (TL) consists to expose a sample to an excitation laser with a Gaussian distribution. Then, the sample absorbs the incident photons and the energy is transformed into heat, generating temperature gradient. This results in a variation of the refractive index of the sample. A second probe laser of lower energy passes through this medium creating a divergent or convergent. This effect is called TL. This signal provides information on the thermal properties of the sample and is widely used for the measurement of the thermal diffusivity of semitransparent samples [22].

The TL experimental setup is shown in Fig. 2. An Ar^+Xe excitation laser with a wavelength of 534 nm and power of 40 mW is focused by a converging lens 1 of 10 cm, a shutter with a time of less than 1 ms, passing through a cuvette (1 cm) where the sample is contained. A second probe He-Ne laser with a wavelength of 632 nm and a power of 1 mW is slightly defocused by a 25 cm lens 2 and passed through the sample [9]. The waist of the probe and the excitation lasers are $\omega_e = 49 \mu\text{m}$ and $\omega_p = 181 \mu\text{m}$. The signal obtained from the sample is collected using a photodiode (Thorlabs) using a spatial filter and a pinhole to ensure that only the signal from the probe laser light is detected and to concentrate the signal in the center of the detector. The signal obtained is recorded and decoded by a Labview software.

In Fig. 3, the typical spectra of the TL signal is shown. The system was calibrated with distilled water with a thermal diffusivity of $14.08 \pm 0.09 \times 10^{-4} \text{ cm}^2/\text{s}$.

From Eq. 1 the TL signal is fitted and the adjustment parameters θ and t_c associated with the photothermal energy and the characteristic time of the formation of the TL are obtained. The photothermal signal as a function of time is given by [22]:

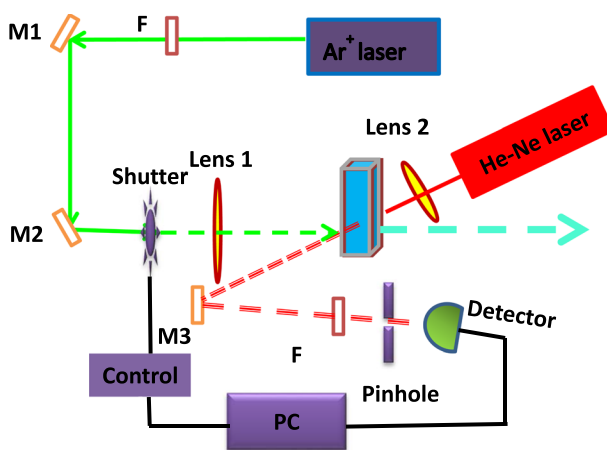


Fig. 2 Experimental set up for mode-mismatched dual-beam TL where F and M are filters and mirrors, respectively

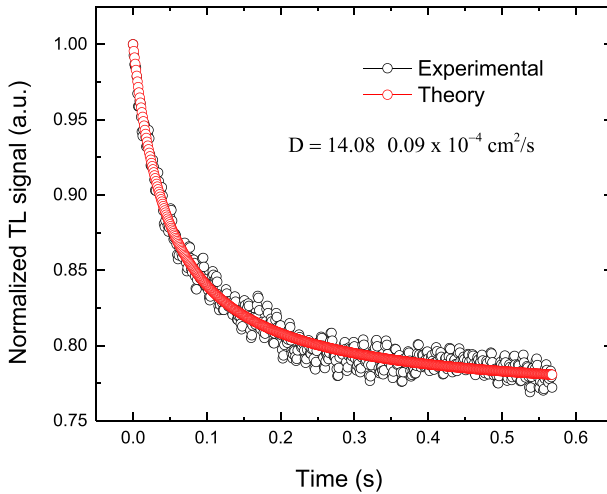


Fig. 3 TL spectra transient for distilled water (prior to the measurements, the system was calibrated with water, with a thermal diffusivity of $14.08 \pm 0.09 \times 10^{-4} \text{ cm}^2 \cdot \text{s}^{-1}$ and the samples were homogenized in an ultrasonic bath for 50 min)

$$I(t) = I_0 \left(1 - \frac{\theta}{2} \tan^{-1} \left(\frac{2mV}{[(1 + 2m)^2 + V^2] \frac{t_c}{2t} + 1 + 2m + V^2} \right) \right)^2 \tag{1}$$

where:

$$m = \left(\frac{\omega_{1p}}{\omega_e} \right)^2 \tag{2}$$

$$\theta = \frac{P_e AL d_n}{k \lambda_p d_T} \tag{3}$$

where $I(t)$ and I_0 are the intensities in the center of the beam at time t and for I ($t=0$) at the initial time, respectively. P_e is the power of the excitation laser, A , L , k , λ_p and d_n/d_T are the absorption of the sample, the length of the quartz cuvette, the thermal conductivity, the wavelength of the probe laser and the coefficient of the refractive index as function of the temperature, respectively; ω_{1p} and ω_e are the ratio of the probe and excitation beam of the sample, respectively. The constant optical parameters were $m = 13.69$ and $V = 1.22$. The time of TL formation for t_c , is calculated as follows:

$$D = \frac{\omega_e^2}{4t_c} (\text{cm}^2 \text{ s}^{-1}) \tag{4}$$

3 Results and Discussion

A Genesis 10 S UV–vis spectrophotometer was used to obtain the UV–visible spectrum of the samples in the range of 190–500 nm, with a step of 5 nm. The GO structural characterization and the morphology and particle size were determined by transmission electron microscopy (TEM). The measurements were made with a JEOL JEM1010 electron microscope with an accelerating voltage of 60 kV. For TEM characterization, a droplet of the nanofluids was placed on carbon-coated copper grid and dried at room temperature. Fourier Transform infrared spectroscopy (FTIR) was used to study the chemical structure and functional groups presents in a range of 400–4000 cm^{-1} with a step of 2 cm^{-1} with a Perkin Elmer spectrometer [23].

UV–Vis spectroscopy spectrum of the graphene oxide nanoparticles dispersions at different concentrations of graphene/water: 0.82 %V, 1.63 %V, 2.43 %V, 3.22 %V, and 4.00 %V is shown in Fig. 4. There are two main absorption peaks, one at 230 nm and another at 303 nm in the UV–visible. The peak at 230 nm is due to π – π^* transition of C–C aromatic bonds for GO and the peak at 303 nm correspond to an n – π^* transition. A shift of the peaks in the visible region is observed. Also, the absorption value increase when increased the concentration of the graphene oxide nanoparticles [24, 25].

TEM images of the particles with a uniform particle size distribution and spherical in shape are shown in Fig. 5 with diameters on the nanometric scale. Based on measurements taken from the TEM micrographs, the size distribution histogram for the samples was obtained (Fig. 5). A Gaussian adjustment with a narrow distribution of diameters with an average particle diameter of 7.4 nm and its size distribution with a standard deviation of 0.8 nm show the homogeneity of

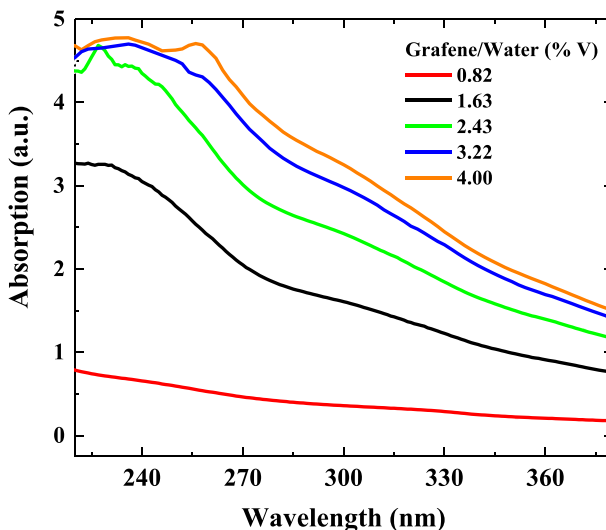


Fig. 4 Optical absorption spectra of GO nanoparticles with %V concentration

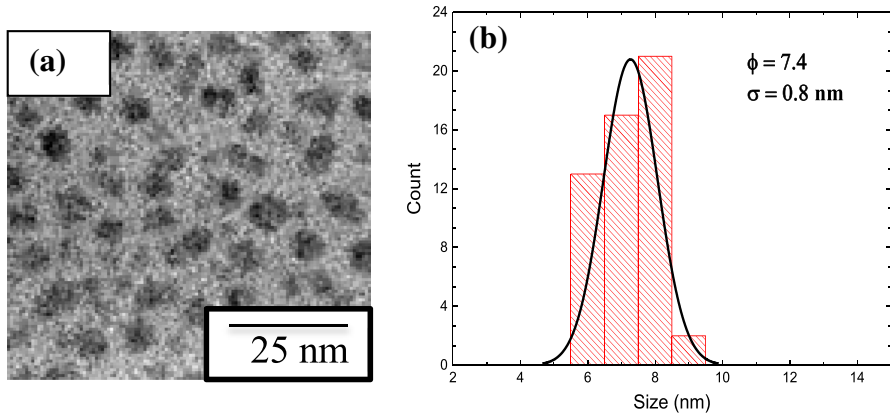


Fig. 5 (a) TEM micrographs; (b) size distribution of graphene oxide particles with an average size of 7.4 nm and standard deviation of 0.8 nm

the diameter of the graphene oxide nanoparticles. The images were analyzed by ImageJ software.

The TL signal for different concentrations of GO is shown in Fig. 6. The continuous line shows the best fit of the Eq. 1 to the experimental data. The adjustment parameters characteristic time t_c and θ were obtained. Using t_c , the thermal diffusivity value was obtained from Eq. 4. θ is proportional to the variation of the refractive index as a function of the temperature (dn/dT) using Eq. 3. For each concentration 0.82 %V, 1.63 %V, 2.43 %V, 3.22 %V and 4.0 %V, the thermal diffusivity values were obtained: $15.02 \pm 0.16 \text{ cm}^2 \cdot \text{s}^{-1}$, $17.07 \pm 0.11 \text{ cm}^2 \cdot \text{s}^{-1}$, $20.53 \pm 0.25 \text{ cm}^2 \cdot \text{s}^{-1}$, $22.65 \pm 0.26 \text{ cm}^2 \cdot \text{s}^{-1}$ and $27.59 \pm 0.51 \times 10^{-4} \text{ cm}^2 \cdot \text{s}^{-1}$, respectively. Distilled water was used for TL system calibration. A thermal diffusivity value of $14.08 \pm 0.09 \times 10^{-4} \text{ cm}^2 \cdot \text{s}^{-1}$ was obtained in agreement with the values reported in the literature [26, 27]. To measure the thermal diffusivity of the water for calibration, a small concentration of R6G (rhodamine) at $0.0024 \text{ mg} \cdot \text{L}^{-1}$ was used to obtain an optimal window in the visible region. Water thermal diffusivity is similar in magnitude to common solvents showing poor thermal blooming effect. A dye such a R6G added to water improves the light absorption without altering the thermal diffusivity of the medium [28, 29]. Table 1 summarizes the results of the concentrations in %V, t_c , θ and the diffusivities obtained by thermal lens.

There was an increase in thermal diffusivity with the concentration in %V of the nanoparticles as seen in Fig. 7. For example, this increase in thermal diffusivity was around 60 % for a 3.22 %V concentration of graphene compared to water at room temperature. Esfahani [17] reported an enrichment of GO nanosheets of 18.9 % for a concentration of 0.1 wt% in water as the base liquid. When increasing the concentration to 0.5 wt%, the enhancement was 19.9%, observing little variation of the enrichment, different to this work. According to Esfahani, the concentration of graphene is not relevant in thermal conductivity measurement. Therefore, in this work it was demonstrated that the concentration of GO is important for diffusivity thermal determination this was relevant, opposite to Esfahani's work. It is known that by the

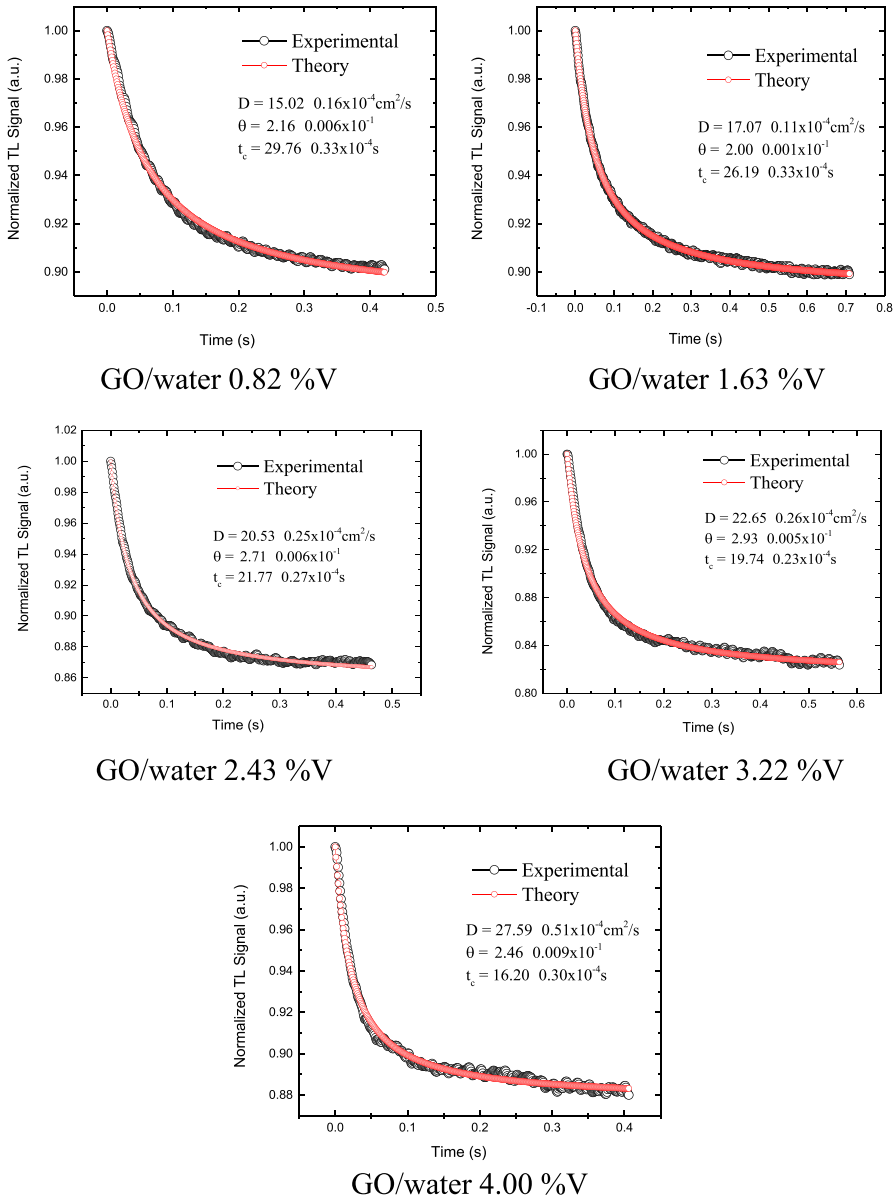


Fig. 6 TL signal for the different GO/water concentrations

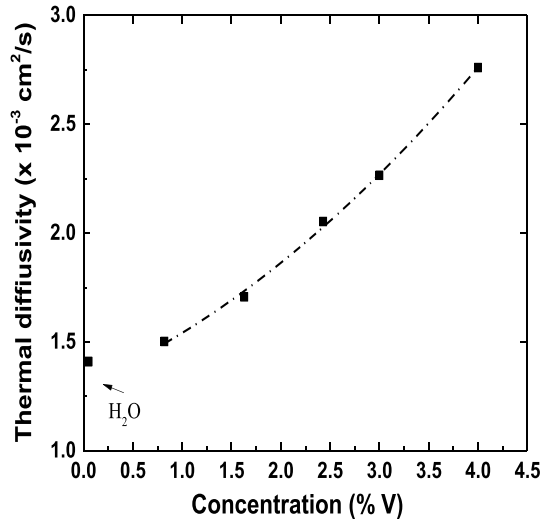
relation $D = k/\rho C_p$ the thermal diffusivity is proportional to the thermal conductivity. If there is an increase in conductivity, the thermal diffusivity increases. Although the density and the heat capacity are involved in the equation, none of them were measured in this work. The product of ρC_p have been defined as the specific volumetric heat capacity of the nanofluid [30]. Authors like Zhou et al., have demonstrated that

Table 1 Thermal parameters, diffusivity and % enhancement for the different concentrations

No.	GO/H ₂ O (%V)	t_c (10^{-4} s)	θ ($\times 10^{-1}$)	D (10^{-4} cm ² /s)	Enhancement (%)
	H ₂ O	28.40 ± 0.22	94.86 ± 0.20	14.08 ± 0.09	
1	0.82	29.76 ± 0.33	2.16 ± 0.006	15.02 ± 0.16	7
2	1.63	26.19 ± 0.17	2.00 ± 0.001	17.07 ± 0.11	22
3	2.43	21.77 ± 0.27	2.71 ± 0.006	20.53 ± 0.25	47
4	3.22	19.74 ± 0.23	2.93 ± 0.005	22.65 ± 0.26	62
5	4.00	16.20 ± 0.30	2.46 ± 0.009	27.59 ± 0.51	95

*The values of t_c and θ were obtained from the theoretical fitting according to Eq. 1 and D from Eq. 4

Fig. 7 Diffusivity thermal enhancement vs %V concentration. The dashed line is a guide for the eye



this specific volumetric heat capacity is almost constant as a function of the volume of the fraction in the nanofluid [31]. The increase in conductivity with an increase in the volume of the fraction have been well demonstrated in the literature [32]. Afrand et al. [33] where it reported for nanoparticles dispersed in different base fluids, an enrichment of 90 % in nanofluids containing Fe₃O₄ nanoparticles in water for a concentration of 3 V%. From the experimental results it can be seen that thermal conductivity is enhanced with an increase in the volume fraction as shown in this work with a value of 95%. Although increasing concentration of nanostructures is known to be effective in enhancing the thermal conductivity of nanofluids, the mechanisms related to this enhancement must be elucidated.

The increase in thermal diffusivity of graphene oxide suspended in water with concentration has been explained due to the following factors which influence the enhancement of thermal diffusivity such as phonons, free electrons, collisions, and molecular diffusivity. If there is an increase in the temperature in the nanofluid, the heat transfer increases due to a greater vibration (phonons), a greater energy of free

electrons and a rapid collision and molecular diffusion induces a higher thermal conductivity, due to the suspension of solid nanoparticles [16, 34].

4 Conclusions

Colloidal suspensions of graphene nanoparticles were prepared using the microwave-assisted hydrothermal method. The thermal diffusivity of nanofluids such as water containing graphene oxide (GO) nanoparticles, was observed to be strongly dependent on the presence of the nanoparticle concentration. The results show that the nanofluid had a substantially increased thermal diffusivity with respect to the base fluid. The diffusivity had an enrichment of 7 % to 95 % for concentrations of 0.82 %V to 4.0 %V. Possible factors for the enrichment of thermal diffusivity are due to phonons, free electrons, collisions, and molecular diffusion of the sample. Possible applications of this work is related to high cooling for devices such as solar cells and in micro-electronics.

Acknowledgments Authors would like to thank CONACYT, COFAA, and CGPI-IPN, Mexico, for their partial financial support. Also, to the Red de Nanofotónica.

References

1. M.V. Marquezini, N. Cella, A.M. Mansanares, H. Vargas, L.C.M. Miranda, *Meas. Sci. Technol.* **2**, 396 (1991)
2. J. Caereles, C. Glorieux, J. Thoen, *Rev. Sci. Ins.* **69**, 2452 (1998)
3. S.M. Shibli, A.L.L. Dantas, A. Bee, *Braz. J. Phys.* **31**(3), 418 (2001)
4. M. Chirtoc, G. Milhailescu, *Phys. Rev. B* **40**, 9606 (1980)
5. R. Carbajal Valdez, J.L. Jiménez-Pérez, A. Cruz Orea, Z.N. Correa Pacheco, M.L. Alvarado Noguez, I.C. Romerolbarra, J.G. Mendoza Álvarez, *Thermochim. Acta* **657**, 66 (2017)
6. G. López-Gamboa, J.L. Jiménez-Pérez, Z.N. Correa-Pacheco, M.L. Alvarado-Noguez, M. Amorin Lima, A. Cruz-Orea, J.G. Mendoza Alvarez, *Int. J. Thermophys.* **41**(10), 1 (2020)
7. N. Sezer, M.A. Atieh, M. Koç, *Powder Technol.* **344**, 404 (2019)
8. X. Liu, Z. Rao, *Thermochim. Acta* **647**, 15 (2017)
9. J.L. Jimenez-Perez, G. Lopez Gamboa, J.F. Sanchez Ramirez, Z.N. Correa-Pacheco, V.E. Lopez Lopez, L. Tepech-Carrillo, *Appl. Phys. A* **122**, 925 (2016)
10. M. Gresil, Z. Wang, Q.A. Poutrel, C. Soutis, *Sci. Rep.* **7**, 1 (2017)
11. Y. Wang, C. Zou, W. Li, Y. Zou, H. Huang, *Int. J. Heat Mass Tran.* **156**(119735), 1 (2020)
12. L.O. Usoltseva, M.V. Korobov, M.A. Proskurnin, *J. Appl. Phys.* **128**(19), 190901 (2020)
13. C. Liu, M. Chen, W. Yu, Y. He, *ES Energy Environ.* **2**, 31 (2018)
14. M. Potenza, A. Cataldo, G. Bovesecchi, S. Corasaniti, P. Coppa, S. Belluci, *AIP Adv.* **7**(075214), 1 (2017)
15. M.R. Rodríguez-Laguna, A. Castro-Alvarez, M. Sledzinska, J. Maire, F. Costanzo, B. Ensing, M. Pruneda, P. Ordejón, C.M. Sotomayor Torres, P. Gómez-Romero, E. Chávez-Ángel, *Nanoscale* **10**, 15402 (2018)
16. N. Ahammed, L. Godson Asirvatham, J. Titus, J. Raja Bose, S. Wongwises, *Int. Commun. Heat Mass* **70**, 66 (2016)
17. M.R. Esfahani, E.M. Languri, M.R. Nouna, *Int. Commun. Heat Mass Transf.* **76**, 308 (2016)
18. S. Vishnuprasad, K. Haribabu, V.T. Perarasu, *Heat Mass Transf.* **55**, 2221 (2019)
19. W. Hummers Jr., R. Offeman, *J. Am. Chem. Soc.* **80**(6), 1339 (1958)
20. H.S. Kim, T.J. Oweida, Y.G. Yingling, *J. Mater. Sci.* **53**, 5766 (2008)
21. M. Drogg, *Dealing with Uncertainties, A Guide to Error Analysis* (Springer, Berlin, 2007).

22. J. Shen, R.D. Lowe, R.D. Swook, *Chem. Phys.* **165**, 385 (1992)
23. J.L. Jiménez-Pérez, R. Gutiérrez-Fuentes, G. López-Gamboa, J.F. Sánchez-Ramírez, Z.N. Correa-Pacheco, R. Carbajal-Valdéz, *Opt. Mater.* **84**, 236 (2018)
24. Q. Lai, S. Zhu, X. Luo, M. Zou, S. Huang, *AIP Adv.* **2**(031146), 1 (2012)
25. T. Emiru, D. Ayele, *Egypt J. Basic Appl. Sci.* **4**, 74 (2017)
26. P.R.B. Pedreira, L. Hirsch, J.R.D. Pereira, A.N. Medina, A.C. Bento, M.L. Baesso, *Rev. Sci. Inst.* **74**, 808 (2003)
27. R.C. Weast, *Handbook of Chemistry and Physics* (CRC Press, Boca Raton, 1987).
28. V.P. Zharov, K.E. Mercer, E.N. Galitovskaya, M.S. Smeltzer, *Biophys. J.* **90**, 619 (2006)
29. V.P. Zharov, D.O. Lapotko, *IEEE J. Sel. Top. Quant. Electron.* **11**, 733 (2005)
30. V.M. Lenart, N.G.C. Astrath, R.F. Turchiello, G.F. Goya, S.L. Gómez, *J. Appl. Phys.* **123**, 085107 (2018)
31. L.P. Zhou, B.X. Wang, X.F. Peng, X.Z. Du, Y.P. Yang, *Adv. Mech. Eng.* **2**, 172085 (2010)
32. R. Bakhtiari, B. Kamkari, M. Afrand, A. Abdollahi, *Powder Technol.* (2021)
33. M. Afrand, D. Toghraie, N. Sina, *Int. Commun. Heat Mass Transf.* **75**, 62 (2016)
34. T. Hong, H. Yang, C. J. Choi, *J. Appl. Phys.* **97**(064311), 1 (2005)

Publisher's Note Springer Nature remains neutral with regard to jurisdictional claims in published maps and institutional affiliations.

Authors and Affiliations

J. L. Jiménez-Pérez¹  · G. López-Gamboa² · J. F. Sánchez-Ramírez³ · Z. N. Correa-Pacheco⁴ · A. Netzahual-Lopantzi¹ · A. Cruz-Orea⁵

- ¹ Unidad Profesional Interdisciplinaria en Ingeniería y Tecnologías Avanzadas-Instituto Politécnico Nacional, Av. IPN, No. 2580, Col. Barrio La Laguna Ticomán, Gustavo A. Madero, C.P. 07340 Mexico, Mexico
- ² Universidad Politécnica del Valle de Toluca, Km 5.6, Carretera Toluca-Almoloya de Juárez, Santiaguito Tlalcalcali, C.P. 50904 Almoloya de Juárez, Mexico
- ³ CIBA-Instituto Politécnico Nacional, Ex-Hacienda San Juan Molino Carretera Estatal Tecuexcomac-Tepetitla Km 1.5, C.P. 90700 Tlaxcala, Mexico
- ⁴ CONACYT-Instituto Politécnico Nacional, Centro de Desarrollo de Productos Bióticos, Carretera Yautepec-Jojutla, km 6, calle CEPROBI No. 8, Col. San Isidro, C.P. 62731 Yautepec, Morelos, Mexico
- ⁵ Departamento de Física, CINVESTAV-IPN, Av. Instituto Politécnico Nacional, No. 2508, Col. San Pedro Zacatenco, Mexico C.P. 07360, México